AGU PUBLICATIONS

Space Weather

RESEARCH ARTICLE

10.1002/2014SW001143

Key Points:
- Fluxes of $E > 2$ MeV electrons at GOES West factor of about 2.5 higher than at GOES East
- Determination of the 1 in 10, 1 in 50, and 1 in 100 year event at GEO
- Largest $E > 2$ MeV flux observed at GEO in 20 years is a 1 in 50 year event

Correspondence to:
N. P. Meredith,
nmer@bas.ac.uk

Citation:
Meredith, N. P., R. B. Horne, J. D. Isles, and J. V. Rodriguez (2015), Extreme relativistic electron fluxes at geosynchronous orbit: Analysis of GOES $E > 2$ MeV electrons, *Space Weather*, *13*, 170–184, doi:10.1002/2014SW001143.

Received 11 NOV 2014
Accepted 13 FEB 2015
Accepted article online 19 FEB 2015
Published online 16 MAR 2015

Extreme relativistic electron fluxes at geosynchronous orbit: Analysis of GOES $E > 2$ MeV electrons

Nigel P. Meredith[1], Richard B. Horne[1], John D. Isles[1], and Juan V. Rodriguez[2,3]

[1]British Antarctic Survey, Natural Environment Research Council, Cambridge, England, [2]Cooperative Institute for Research in Environmental Sciences, University of Colorado Boulder, Boulder, Colorado, USA, [3]National Geophysical Data Center, National Oceanic and Atmospheric Administration, Boulder, Colorado, USA

Abstract Relativistic electrons ($E > 1$ MeV) cause internal charging on satellites and are an important space weather hazard. A key requirement in space weather research concerns extreme events and knowledge of the largest flux expected to be encountered over the lifetime of a satellite mission. This is interesting both from scientific and practical points of view since satellite operators, engineers, and the insurance industry need this information to better evaluate the effects of extreme events on their spacecraft. Here we conduct an extreme value analysis of daily averaged $E > 2$ MeV electron fluxes from the Geostationary Operational Environmental Satellites (GOES) during the 19.5 year period from 1 January 1995 to 30 June 2014. We find that the daily averaged flux measured at GOES West is typically a factor of about 2.5 higher than that measured at GOES East, and we conduct independent analyses for these two locations. The 1 in 10, 1 in 50, and 1 in 100 year daily averaged $E > 2$ MeV electron fluxes at GOES West are 1.84×10^5, 5.00×10^5, and 7.68×10^5 cm^{-2} s^{-1} sr^{-1}, respectively. The corresponding fluxes at GOES East are 6.53×10^4, 1.98×10^5, and 3.25×10^5 cm^{-2} s^{-1} sr^{-1}, respectively. The largest fluxes seen during the 19.5 year period on 29 July 2004 were particularly extreme and were seen by satellites at GOES West and GOES East. The extreme value analysis suggests that this event was a 1 in 50 year event.

1. Introduction

Space weather is an increasingly important natural hazard risk as society becomes ever more heavily dependent on satellite technology for communications, navigation, defense, and Earth observation [e.g., *Horne et al*., 2013]. The concern at government level in the UK is such that space weather was added to the UK National Risk Register of Civil Emergencies in 2012. The relative likelihood of extreme space weather occurring in the next 5 years is significant and has been estimated as between 1 in 2 and 1 in 20 [*Cabinet Office*, 2012]. In Europe, space weather is recognized as a threat to its critical infrastructure [*Krausmann*, 2011] and is a priority for European Space Agency's Space Situational Awareness program. Following President Obama's meeting with Prime Minister David Cameron in 2011, space weather is also a topic of special collaboration between the UK and the U.S [*Viereck*, 2012].

The impacts of space weather on satellite operations range from momentary interruptions of service to a total loss of capabilities when a satellite fails. For example, during the 2003 Halloween geomagnetic storms 47 satellites experienced anomalies, while one satellite, the Japanese/U.S. U.S. $640 million Midori 2 environmental research satellite, was a complete loss [*Webb and Allen*, 2004]. Other satellite losses and partial losses that have been associated with adverse space weather conditions include Anik E2 on 20 January 1994 [*Baker*, 2001], Telstar 401 on 11 January 1997 [*Lanzerotti et al.*, 1998], Galaxy 10R on 3 August 2004 [*Choi et al.*, 2011], Intelsat 804 on 14 January 2005 [*Royal Academy of Engineering Report*, 2013], and Galaxy 15 on 5 April 2010 [*Allen*, 2010]. One recent report estimates that the loss of revenue from satellite services alone, for an event 3 times the size of the Carrington event of 1859, could be as high as U.S. $30 billion [*Odenwald and Green*, 2007]. However, there is a large uncertainty associated with this estimate, and the likely effect of a severe space weather storm on the satellite fleet remains difficult to quantify.

Space weather can affect satellites in a number of ways. For example, galactic cosmic rays, which vary in antiphase with the solar cycle, cause single-event upsets [e.g., *Wilkinson et al*., 1991]. Solar energetic protons, which are associated with coronal and/or interplanetary shock waves driven by coronal mass ejections, cause single-event upsets [*Adams et al.*, 1996] and also displacement damage in electronic components. The latter leads to degradation of solar array power over the course of the satellite lifetime. Energetic electrons

affect satellites in two important ways. Suprathermal electrons, with energies of the order of tens of keV, which are injected into the inner magnetosphere during storms and substorms [e.g., *Cayton et al*., 1989], cause surface charging [*Lanzerotti et al.*, 1998; *Koons and Fennell*, 2006] which can damage surface materials and underlying components. At higher energies, relativistic electrons, with energies of the order of 1 MeV and above, cause internal charging [e.g., *Wrenn*, 1995; *Wrenn et al*., 2002; *Gubby and Evans*, 2002], the subsequent discharge of which can lead to component failure and trigger phantom commands.

Relativistic electrons (E >1 MeV) are a major and well-established cause of radiation damage to satellites in Earth's orbit. These so-called "killer" electrons reside in two distinct regions known as the Earth's inner and outer Van Allen radiation belts [*Van Allen and Frank*, 1959]. The inner radiation belt, which lies between L = 1.1 and 2, is relatively stable, except during the largest geomagnetic storms [*Baker et al.*, 2007]. Here L is the distance in Earth radii to the equatorial crossing of a given geomagnetic field line. In contrast, the outer radiation belt, which typically lies between L = 3 and L = 7, is highly dynamic. In this region the flux of relativistic electrons can vary by orders of magnitude on timescales ranging from minutes to weeks [*Blake et al.*, 1992; *Baker et al.*, 1994]. This variability is caused by a variety of transport, acceleration, and loss processes [e.g., *Horne*, 2002; *Thorne*, 2010], all of which tend to be enhanced during enhanced geomagnetic activity which is ultimately driven by the Sun. Relativistic electrons can penetrate through satellite surface material and may deposit their charge on insulators or on ungrounded conductors. This charge can build up over time leading to arcing or electrostatic discharge which can damage components and, in extreme cases, even prove fatal for a satellite. Relativistic electrons also pose a risk to astronauts on extravehicular activities [e.g., *Dacheva et al*., 2013].

Geosynchronous orbit is a low-inclination orbit around the Earth with an orbital period equal to the Earth's sidereal rotation period. It is a particularly important region both for communications and weather satellites, since satellites located in this orbit remain in the same area of the sky as viewed from the Earth, staying within view of a given ground station. As of May 2012, there were 419 satellites in geosynchronous orbit, representing about 42% of the entire satellite fleet [*Horne et al.*, 2013]. Geosynchronous satellites operate at an altitude of approximately 35,790 km in the Earth's geographic equatorial plane corresponding to L = 6.6. Geosynchronous orbit is thus located toward the edge of the outer radiation belt, and so geosynchronous satellites are exposed to relativistic electrons. Indeed, there is a significant correlation between satellite anomalies and the E > 2 MeV electron flux at geosynchronous orbit [*Wrenn*, 1995; *Iucci et al.*, 2005].

The service life expectancy of a modern communications satellite at geosynchronous orbit is typically 10 to 15 years. Satellite operators and engineers are, therefore, interested in extreme events that occur on these and longer timescales. In particular, they need to know the 1 in 10, 1 in 50, and 1 in 100 year fluxes of relativistic electrons to try and assess how hostile the radiation belt environment can become in a worst-case scenario. Such information can be used to help assess the impact of extreme events on the satellite fleet and to help improve the resilience of future satellites by better design of satellite components if required. Satellite insurers are also interested in extreme events to help them evaluate realistic disaster scenarios.

In this study we use nearly 20 years of data from the National Oceanic and Atmospheric Administration (NOAA) Geostationary Operational Environmental Satellites (GOES) to determine the number of times the flux of E > 2 MeV electrons rises above given thresholds and to determine probability distributions. We also conduct an extreme value analysis to determine the 1 in 10, 1 in 50, and 1 in 100 year flux levels. The instrumentation and data analysis are described in section 2, and the probability distributions are presented in section 3. In section 4 we present a detailed case study, featuring the largest event recorded in our study period. The extreme value analysis is then described and the results are presented in section 5. Finally, the results are discussed and the conclusions are presented in sections 6 and 7, respectively.

2. Instrumentation and Data Analysis

In this study we use particle data from the energetic particle sensors (EPS) on board the NOAA GOES satellites. These satellites operate at geosynchronous orbit at an altitude of approximately 35,790 km. Here we use data from GOES 8–13 and 15 covering the interval from 1 January 1995 to 30 June 2014.

The E > 2 MeV electron flux is measured by a wide-aperture dome detector assembly with a field of view of about 60° by 120° [*Onsager et al.*, 1996]. The dome detectors on GOES 8, 9, 11, and 12 are mounted such that

Table 1. Satellite Data Used in Study

	Dates
GOES East	
GOES 8	18 Feb 1995 to 9 May 2003
GOES 12	1 Oct 2003 to 28 Nov 2008
GOES 13	1 May 2010 to date
GOES West	
GOES 9	2 Apr 1996 to 27 Jul 1998
GOES 10	17 Aug 1998 to 21 Jun 2006
GOES 11	22 Jun 2006 to 27 Feb 2011
GOES 15	7 Dec 2011 to date

their fields of view look westward, whereas the dome detector on GOES 10 looks eastward. There are two sets of dome detectors on GOES 13 and 15, one set looking westward and the other eastward, depending on the orientation of the spacecraft [*Rodriguez et al.*, 2014]. For our study we select the measurements from the westward facing detector. Some of the archived data have invalid position information. When this occurs, we interpolate from the known positions of the satellite.

In this study we focus on the largest fluxes of $E > 2$ MeV electrons observed by the GOES satellites. However, at the highest flux levels, the output rate of a given instrument can be significantly lower than the true rate owing to the effect of dead time. The dead time is the period initiated by the onset of a charge pulse from an incident particle during which a subsequent pulse cannot be measured. A nonextendable (nonparalyzable) dead time correction [*ICRU*, 1994; *Knoll*, 2000] was recommended by the builder of the GOES 13–15 EPS [*Hanser*, 2011]. The multiplicative nonextendable dead time correction is given by

$$\eta = \frac{1}{1 - \tau \Sigma_{i=1}^{N} R_i} \tag{1}$$

where τ is the dead time (2.5 μs for EPS) and R_i are the coincidence rates from the set of channels measured by a given instrument. Since the detector and electronic coincidence logic designs are identical for the two series, the GOES 13–15 dead time correction is also valid for the GOES 8–12 EPS. The $E > 2$ MeV electrons are measured by the D3 dome detector, along with the $E > 0.8$ MeV electrons, the 15–40 MeV protons, and the 60–160 MeV alpha particles. The D3 dome dead time correction is dominated by the $E > 0.8$ MeV rates, although all four channels contribute, and in the absence of solar energetic particle fluxes, it can be estimated accurately using only the $E > 0.8$ MeV and $E > 2$ MeV rates. The real-time processing of the GOES 8–15 EPS data has not used a dead time correction. Therefore, in order to have a more accurate estimate of extreme relativistic electron fluxes for this study, the dead time correction has been applied for the first time to the EPS relativistic electron fluxes. Since the focus of this study are extreme events, we apply the correction to days with daily averaged fluxes of $E > 2$ MeV electrons greater than 5000 cm^{-2} s^{-1} sr^{-1} . The dead time correction factor ranges from 1.0 to 1.15 for fluxes near 5000 cm^{-2} s^{-1} sr^{-1} to a factor of ~2 for the highest fluxes observed.

The GOES satellites operate at two primary geographic longitudes, referred to as GOES West and GOES East, located at 135° and 75° W respectively in the Earth's geographic equatorial plane. Due to the Earth's dipole tilt satellites at these two locations operate at different magnetic latitudes with GOES West and GOES East located roughly 4° and 11°N of the magnetic equator, respectively. The satellites are thus located on different L shells with GOES East typically being of the order of 0.2L farther from the Earth. Since the radial gradient of flux is generally outward near geosynchronous orbit, GOES West will typically measure larger fluxes than GOES East [*Onsager et al.*, 2004], and we therefore conduct our analysis for the satellites at GOES West and GOES East separately. For this study a satellite is defined to be at GOES West when its geographic longitude, ϕ, lies in the range $130° < \phi < 140°$W and at GOES East when its geographic longitude lies in the range $70° < \phi < 80°$W. Data collected at other longitudes are not included in the study. The satellites used here, together with the intervals for which they record fluxes of $E > 2$ MeV electrons at GOES West and GOES East, are tabulated in Table 1.

We exclude data recorded by GOES 10 in February 2010 during a period of anomalously low fluxes attributed to count rates which had not been properly converted to fluxes [*Su et al.*, 2014]. We also exclude data from GOES 12 collected in September 2003 due to an offset of 1.5 days between the 5 min and 1 min averages and after 28 November 2008 due to a partial failure of the dome detector. A second period of anomalously low fluxes recorded by GOES 12 in May 2003 is automatically excluded from the analysis since GOES 12 was located at an intermediate longitude during this period.

The $E > 2$ MeV electron fluxes may be contaminated by solar proton events, and measurements made during these events are, therefore, excluded from the analysis. We adopt the NOAA Space Weather

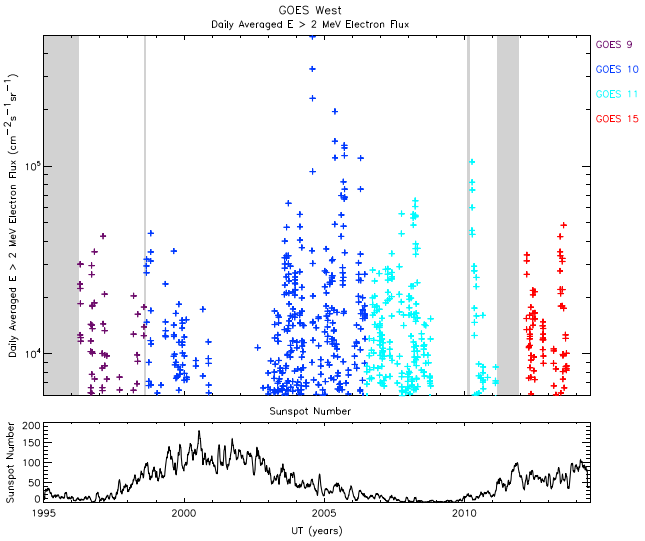

Figure 1. (top) Plot of the daily averaged, dead time-corrected $E > 2$ MeV electron flux measured by GOES satellites at the GOES West location as a function of UT, together with a trace of the (bottom) 27 day averaged sunspot number. The points are color coded to denote the GOES satellite that made the measurement. Periods with no data coverage are shaded grey.

Prediction Center's definition of a solar proton event and exclude the electron data whenever the flux of $E > 10$ MeV protons determined from the GOES EPS measurements is greater than 10 cm^{-2} s^{-1} sr^{-1}. We subsequently calculate the daily average for a given satellite and a given day whenever greater than 90% of the day has good quality data in the absence of a solar proton event. In total, there are 5844 good quality daily data points at GOES West and 5649 good quality data points at GOES East, corresponding to approximately 16 and 15.5 years of operational data, respectively. We emphasize that the good quality data points include daily averaged fluxes both above and below 5000 cm^{-2} s^{-1} sr^{-1} but only fluxes above 5000 cm^{-2} s^{-1} sr^{-1} have been corrected for dead time.

3. Daily Statistics

The daily averaged, dead time-corrected $E > 2$ MeV electron flux at the GOES West position is plotted as a function of UT in Figure 1 (top), together with a trace of the 27 day averaged sunspot number (bottom). Each point represents 1 day, and the data are color coded according to the satellite that made the measurement. Periods when no data are available are shaded grey. The largest fluxes are seen during the declining phase of the solar cycle consistent with previous findings [*Koons*, 2001; *Miyoshi et al.*, 2004]. Flux levels of 10^4, 2×10^4, and 5×10^4 cm^{-2} s^{-1} sr^{-1} were exceeded on 404, 162, and 31 days, respectively.

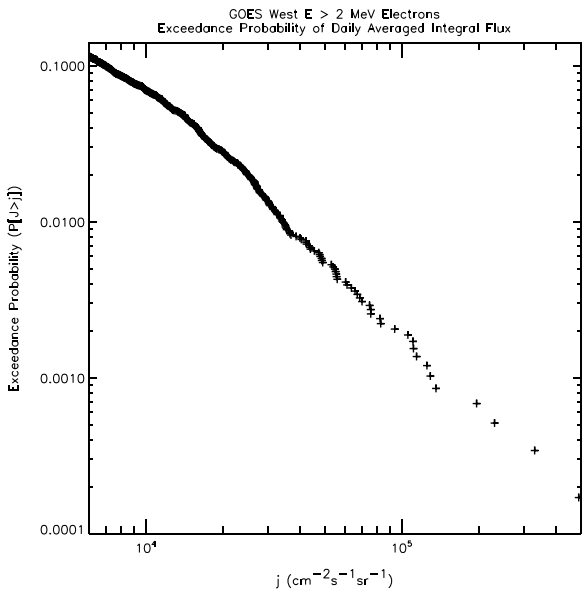

Figure 2. Plot of the exceedance probability of the daily average flux of $E > 2$ MeV electrons measured by the GOES satellites at the GOES West location.

The distribution of the flux of $E > 2$ MeV electrons is shown in Figure 2. To highlight the extremes, we express the distribution as the exceedance probability, $P[J > j]$, which represents the probability that an individual sample, J, exceeds a threshold j. The flux levels that are exceeded 5%, 1%, and 0.1% of the time are 1.35×10^4, 3.41×10^4, and 1.29×10^5 cm^{-2} s^{-1} sr^{-1}, respectively.

The daily averaged, dead time-corrected $E > 2$ MeV electron flux is plotted as a function of UT for the satellite at GOES East, together with a trace of the 27 day averaged sunspot number, in Figure 3 in the same format as Figure 1. Flux levels of 10^4, 2×10^4, and 5×10^4 cm^{-2} s^{-1} sr^{-1} were exceeded on 114, 30, and 3 days, respectively.

The distribution of the flux of $E > 2$ MeV electrons is shown in Figure 4 in the

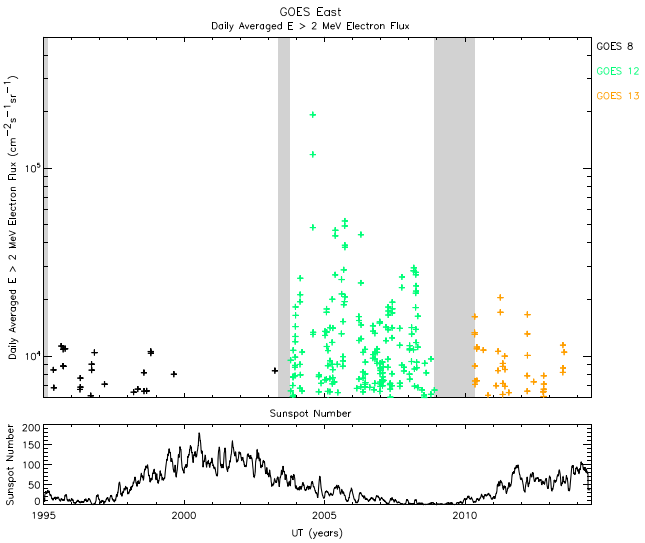

Figure 3. (top) Plot of the daily averaged, dead time-corrected $E > 2$ MeV electron flux measured by GOES satellites at the GOES East location as a function of UT, together with a trace of the (bottom) 27 day averaged sunspot number. The points are color coded to denote the GOES satellite that made the measurement. Periods with no data coverage are shaded grey.

same format as Figure 2. The red symbols represent the exceedance probability measured at GOES West and illustrate that on average, the flux of $E > 2$ MeV electrons measured at GOES East is typically a factor of ~2.5 lower than that measured at GOES West. The flux levels that are exceeded 5%, 1%, and 0.1% of the time are 5.65×10^3, 1.43×10^4, and 4.67×10^4 cm^{-2} s^{-1} sr^{-1}, respectively.

The 10 largest daily averaged fluxes of $E > 2$ MeV electrons observed by satellites at GOES West and GOES East are tabulated in Table 2. This table differs from that published in *Kataoka and Miyoshi* [2008a] in a number of ways. First, the data have been corrected for dead time; second, we create two independent lists, one for the satellite at GOES West and the other for the satellite at GOES East; and third, we choose to tabulate the top 10 daily averages as opposed to the top 10 event maxima. The largest daily averaged flux of $E > 2$ MeV electrons observed at GOES West was 4.92×10^5 cm^{-2} s^{-1} sr^{-1} on 29 July 2004. The satellite at GOES East also recorded its largest flux of 1.93×10^5 cm^{-2} s^{-1} sr^{-1} on the same day. These two independent observations of the most extreme flux suggest that the event was real and captured by both satellites. The largest three fluxes observed at GOES West occurred on three consecutive days illustrating that there is a tendency for the data to cluster in that if the flux is high on a given day, it may also be high on the next day.

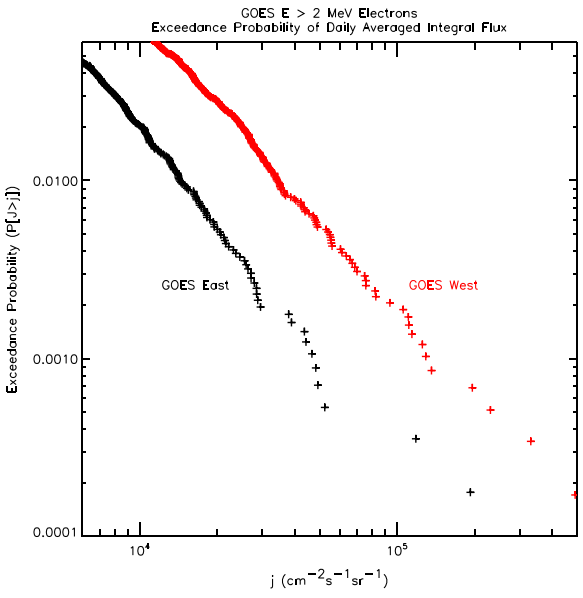

Figure 4. Plot of the exceedance probability of the daily average flux of $E > 2$ MeV electrons measured by the GOES satellites at the GOES East location (black symbols). The exceedance probabilities of the daily average flux of $E > 2$ MeV electrons measured by the GOES satellites at the GOES West location are shown for comparison (red symbols).

4. Case Study

The flux of $E > 2$ MeV electrons for July and August 2004, which includes the interval containing the largest daily averaged fluxes observed during the interval under study, is shown in Figure 5. For this specific interval we corrected all of the $E > 2$ MeV electron data for dead time. During this period the electron fluxes at GOES East were made by GOES 12 and those at GOES West by GOES 10. With the failure of the two highest energy proton channels, GOES 12 data were not used to calculate integral proton fluxes, and the proton fluxes during this interval were provided by GOES 10 and GOES 11 which was located around 105°W. Figure 5 shows (a) the $E > 2$ MeV electron flux, (b) the $E > 10$ MeV integral proton flux, (c) the geographic longitudes, (d) the solar wind speed and IMF *Bz*, (e) the *Dst* index (color coded) together with a trace of the solar wind pressure, and (f) the *Kp* index (color coded) together with a trace of the

Table 2. Largest Daily Averaged $E > 2$ MeV Fluxes Observed at GOES West and GOES East

GOES West		GOES East	
Flux (cm^{-2} s^{-1} sr^{-1})	Date	Flux (cm^{-2} s^{-1} sr^{-1})	Date
4.92×10^5	29 Jul 2004	1.93×10^5	29 Jul 2004
3.31×10^5	28 Jul 2004	1.18×10^5	30 Jul 2004
2.31×10^5	30 Jul 2004	5.24×10^4	19 Sep 2005
1.96×10^5	18 May 2005	4.93×10^4	18 Sep 2005
1.36×10^5	17 May 2005	4.83×10^4	31 Jul 2004
1.29×10^5	17 Sep 2005	4.67×10^4	19 May 2005
1.25×10^5	18 Sep 2005	4.43×10^4	17 Apr 2006
1.14×10^5	19 Sep 2005	4.37×10^4	18 May 2005
1.11×10^5	19 May 2005	3.89×10^4	20 Sep 2005
1.11×10^5	17 Apr 2006	3.79×10^4	21 Sep 2005

AE index. In Figure 5a the 5 min resolution $E > 2$ MeV fluxes are plotted as small dots and the daily averaged $E > 2$ MeV fluxes are shown as large crosses. This period contains an interval with three consecutive geomagnetic storms with *Dst* minima of −99, −136, and −170 nT on 23, 25, and 27 July, respectively (Figure 5e). The storms were each associated with high levels of geomagnetic activity as monitored by the *Kp* and *AE* indices (Figure 5f). Each storm was also associated with strong southward IMF *Bz* and elevated solar wind speeds ($v > 500$ km s^{-1}) (Figure 5d). Following the first storm on the 23 July, the daily averaged flux of $E > 2$ MeV electrons observed by GOES 10 increased by over an order of magnitude to greater than 10^4 cm^{-2} s^{-1} sr^{-1}. A solar proton event hits the Earth on 25 July and lasted until 27 July (Figure 5b). The interval, which is greyed out in Figures 5a and 5b, prevented measurements of the daily averaged flux for three consecutive days. Following the third geomagnetic storm on 27 July, the daily averaged flux of $E > 2$ MeV electrons observed by GOES 10 exceeded 10^5 cm^{-2} s^{-1} sr^{-1} on 28, 29, and 30 July, with a peak flux of 4.92×10^5 cm^{-2} s^{-1} sr^{-1} on 29 July. The flux then remained elevated above 10^4 cm^{-2} s^{-1} sr^{-1} for a further 6 days.

5. Extreme Value Analysis

The main purpose of this study is to determine the extreme values of the daily averaged flux of $E > 2$ MeV electrons that might be encountered by a satellite at geosynchronous orbit. In particular, we would like to know the largest flux that might be observed at this location over a given period of time, namely, in 10, 50, and 100 years. For our study we have roughly 16 years of good quality data, so we need a method to determine the 1 in 50 and 1 in 100 year events. This requires a different statistical approach to that used traditionally to calculate, for example, the mean, standard deviation, and percentiles of a distribution. In this case we use a different branch of statistics known as extreme value analysis. There are two main methods for extreme value analysis; one involves block maxima and the other involves exceedances over a high threshold. One of the objectives of this study is to update and extend the work of *Koons* [2001] who performed an extreme value analysis on the GOES $E > 2$ MeV electrons from 1986 to 1999. For his study *Koons* [2001] chose the exceedances over a threshold approach, and to facilitate comparison with this study, we adopt the same method here. For this approach, also known as the Peaks Over Threshold method, the appropriate distribution function is the generalized Pareto distribution (GPD), first introduced by *Picklands* [1975]. This approach has been used successfully in many fields to estimate, for example, extremes of rainfall [e.g., *Li et al*., 2005], surface temperature [e.g., *Nogaj et al*., 2006], wind speed [e.g., *Della-Marta et al*., 2009], geomagnetic activity [*Thomson et al*., 2011], and storm surge [e.g., *Tebaldi et al*., 2012].

Following *Coles* [2001], the GPD, $G(y)$, may be written in the form

$$G(y) = 1 - \left(1 + \frac{\xi y}{\sigma}\right)^{-\frac{1}{\xi}} \tag{2}$$

where $y = (x - u)$ are the exceedances and x are the data values above the chosen threshold, u. The GPD is characterized by two parameters, a shape parameter, ξ, which controls the behavior of the tail of the distribution and a scale parameter, σ, which determines the statistical dispersion of the distribution. If

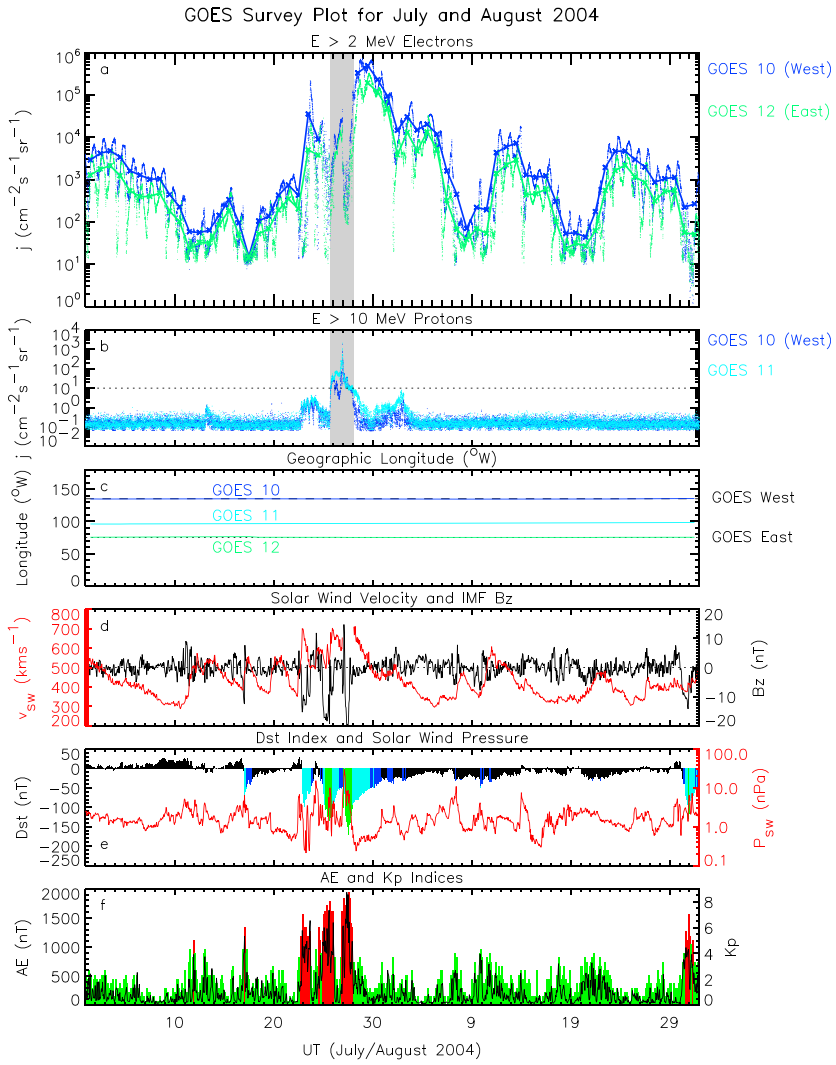

Figure 5. Summary plot of the GOES data for the period July–August 2004. Shown are (a) the $E > 2$ MeV electron flux, (b) the $E > 10$ MeV proton flux, (c) the geographic longitude of the satellites, (d) the solar wind speed and IMF *Bz*, (e) the *Dst* index (color coded) together with a trace of the solar wind pressure, and (f) the *Kp* index (color coded) together with a trace of the *AE* index.

$\xi < 0$, the distribution of exceedances has an upper bound, whereas if $\xi > 0$, the distribution has no upper limit. The GPD is a distribution function, with $1 - G(y)$ representing the probability that a random variable X exceeds some value x given that it already exceeds a threshold u, $P(X > x|X > u)$.

We may assess the quality of a fitted GPD model by comparing the empirical and modeled probabilities and quantiles [*Coles*, 2001]. For probabilities we plot the modeled probability, $G(y)$ against the empirical probability, that X exceeds some value x given that it already exceeds a threshold u. Assuming threshold exceedances $y(1) \leq .. \leq y(k)$ and an estimated model G, the probability plot consists of the pairs

$$\left(\frac{i}{k+1}, G(y_{(i)})\right); i = 1, ..., k \tag{3}$$

For the quantiles, we plot the modeled exceedances against the empirical exceedances, y. The quantile plot consists of the pairs

$$\left(G^{-1}\left(\frac{i}{k+1}\right), y_{(i)} + u\right); i = 1, ..., k \tag{4}$$

where

$$G^{-1}(y) = u + \frac{\sigma}{\xi}((1-y)^{-\xi} - 1) \tag{5}$$

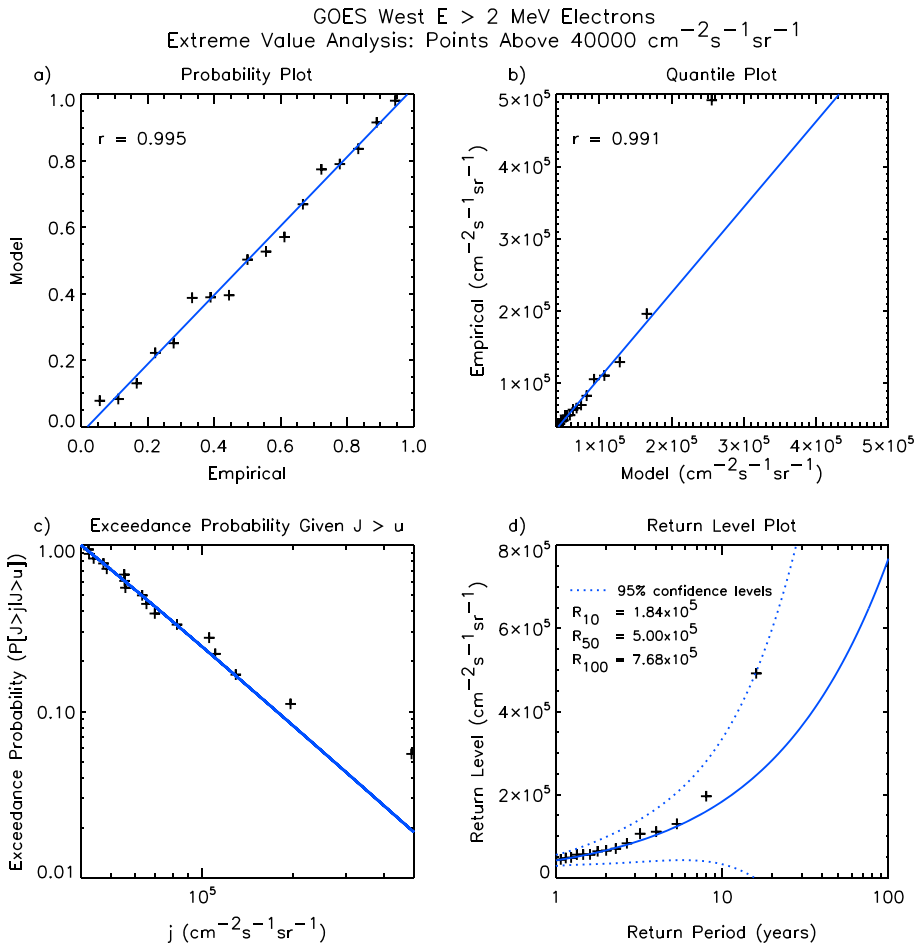

Figure 6. Extreme value analysis for the daily averaged $E > 2$ MeV electron flux measured by GOES satellites at the GOES West location. (a) Probability plot, (b) quantile plot, (c) the exceedance probability given $J > u$, and (d) the return level plot.

If the generalized Pareto model is a good method for modeling the exceedances, y, then both the probability and quantile plots should be approximately linear.

We are primarily interested in the largest flux that is likely to be observed over a given period of time. Following *Coles* [2001], the level, x_N, which is exceeded on average once every N years is given by

$$x_N = u + \frac{\sigma}{\xi}\left((Nn_d\zeta_u)^{\xi} - 1\right) \tag{6}$$

where ζ_u is the probability of an individual observation exceeding the threshold and $n_d = 365.25$ and is the average number of days in any given year. A plot of x_N against N is known as a return level plot.

The data in Table 2 reveal and the plot in Figure 5 shows that there is a tendency for the data to cluster in that a day of high fluxes is likely to be succeeded by another. This breaks an important assumption used in the statistical analysis, namely, that the individual exceedances should be independent [*Coles*, 2001]. The most widely adopted technique for dealing with this issue is known as declustering. We reanalyze the data and bin the groups of the days when the threshold is exceeded into clusters, including periods when the threshold is only exceeded on 1 day. We then identify the cluster maxima and assume that the cluster maxima are independent with conditional exceedances given by the GPD. Here we use an empirical rule to determine clusters of exceedances and consider a cluster to be active until the three consecutive daily averages fall below our chosen threshold. We then fit the GPD to the cluster maxima. In this case ζ_u in equation (5) is given by n_c/n_{tot} where n_c is the number of clusters and n_{tot} the total number of daily values [*Coles*, 2001].

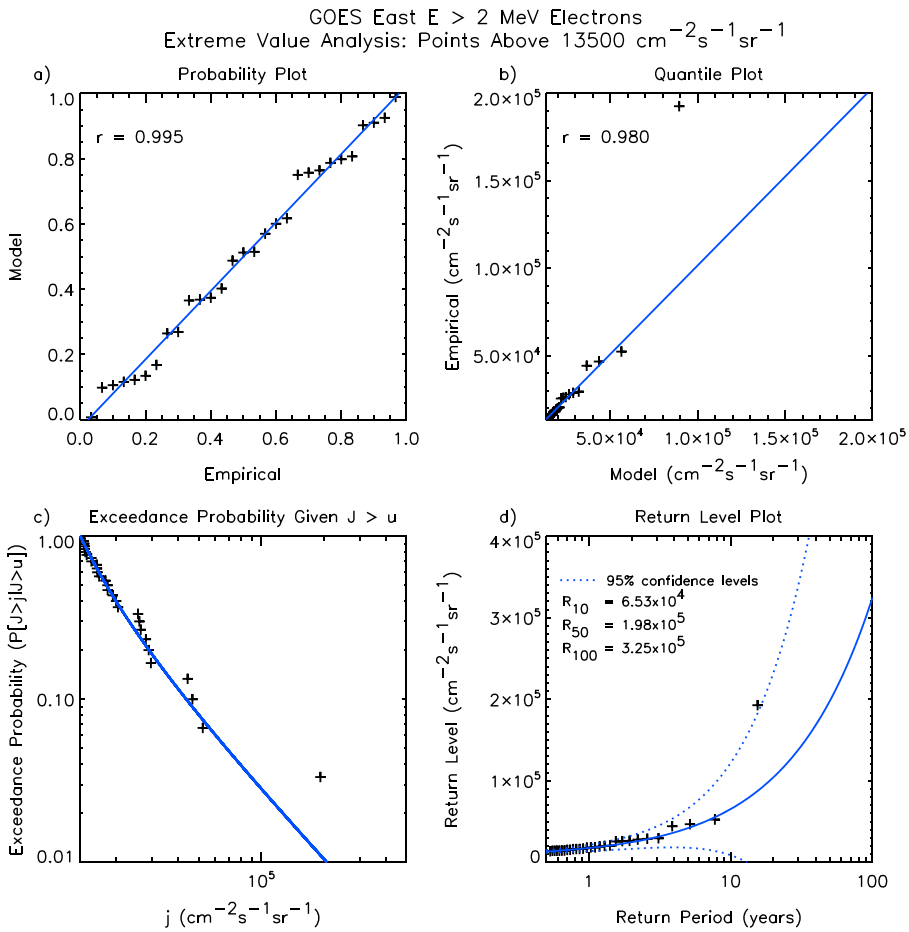

Figure 7. Extreme value analysis for the daily averaged $E > 2$ MeV electron flux measured by GOES satellites at the GOES East location. (a) Probability plot, (b) quantile plot, (c) the exceedance probability given $J > u$, and (d) the return level plot.

For a given threshold we fit the GPD to the cluster maxima by maximum likelihood estimation using the routine gpd.fit provided in the library ismev [*Heffernan et al.*, 2014] of the R statistical language [*R Development Core Team*, 2008].

To determine appropriate thresholds, we examined the quantile plots for the dead time-corrected fluxes at GOES West and GOES East. The quantile plots became approximately linear for fluxes greater than 4.0×10^4 and 1.35×10^4 cm^{-2} s^{-1} sr^{-1} at GOES West and East, and we, therefore, chose these values as the respective thresholds. The numbers of individual observations that exceed these threshold values are 45 and 66 at GOES West and East, respectively. When the data are declustered, the numbers of clusters that exceed these limits are 17 and 29 at GOES West and GOES East, respectively, illustrating the importance of declustering in this study.

For the data collected at GOES West the maximum likelihood estimates of the scale and shape parameters are $(2.6 \pm 1.5) \times 10^4$ and 0.61 ± 0.44, respectively. Here and elsewhere the quoted error is the standard error. The shape parameter is positive suggesting that the distribution has no upper limit. The probability plot, showing the modeled and empirical probabilities, for the cluster maxima of $E > 2$ MeV electrons at GOES West is shown in Figure 6a. The blue line represents the best fit straight line to the data points using simple linear regression and has a correlation coefficient of 0.995. The corresponding quantile plot, showing the empirical and modeled quantiles, for the cluster maxima of $E > 2$ MeV electrons at GOES West is shown in Figure 6b. Excluding the outlier with a measured flux of 4.92×10^5 cm^{-2} s^{-1} sr^{-1}, the blue line represents the best fit straight line to the data using simple linear regression and has a correlation coefficient of 0.991. Both fits are approximately linear illustrating that the generalized Pareto model is a good method for modeling

the exceedances at GOES West. The exceedance probability of the cluster maxima above the threshold value of 4.0×10^4 cm^{-2} s^{-1} sr^{-1} ($P[J > j|J > u]$) is shown in Figure 6c (black symbols), together with the maximum likelihood fit (blue line). The return level plot, showing the level that is exceeded on average once every N years as a function of N, for the declustered GOES West $E > 2$ MeV electron flux is shown in Figure 6d. The symbols represent the experimental return levels, and the solid blue line represents the 1 in N year return level determined from equation (5). The dotted blue lines represent the 95% confidence interval of the 1 in N year return level. The 1 in 10, 1 in 50, and 1 in 100 year daily averaged $E > 2$ MeV electron fluxes at GOES West are 1.84×10^5, 5.00×10^5, and 7.68×10^5 cm^{-2} s^{-1} sr^{-1}, respectively.

The analysis was repeated for the data at GOES East. At this location the maximum likelihood estimates of the scale and shape parameters are $(5.0 \pm 1.8) \times 10^3$ and 0.73 ± 0.33, respectively. The shape parameter is positive again suggesting that the distribution has no upper limit. The probability plot for the cluster maxima of $E > 2$ MeV electrons at GOES East is shown in Figure 7a, in the same format as Figure 6a. The correlation coefficient for the fit is 0.995. The corresponding quantile plot for the cluster maxima of $E > 2$ MeV electrons at GOES West is shown in Figure 7b, in the same format as Figure 6a. Excluding the outlier with a measured flux of 1.93×10^5 cm^{-2} s^{-1} sr^{-1}, the correlation coefficient for the fit is 0.980. Both fits are approximately linear, illustrating that the generalized Pareto model is also a good method for modeling the exceedances at GOES East. The exceedance probability of the cluster maxima above the chosen threshold of 1.35×10^4 cm^{-2} s^{-1} sr^{-1} (black symbols) together with the fit to the data (blue line) is shown in Figure 7c. The return level plot for the declustered GOES East $E > 2$ MeV electron flux is shown in Figure 7d in the same format as Figure 6d. The 1 in 10, 1 in 50, and 1 in 100 year daily averaged $E > 2$ MeV electron fluxes at GOES East are 6.53×10^4, 1.98×10^5, and 3.25×10^5 cm^{-2} s^{-1} sr^{-1}, respectively.

6. Discussion

The daily averaged flux measured at GOES West is typically a factor of ~2.5 higher than that measured at GOES East. This difference is large compared with the average offsets between the various instruments of the order of 20–30% as discussed in the appendix. The difference is largely due to the fact that GOES West and GOES East, which operate at 135° and 75°W, respectively, are located at different magnetic latitudes and hence at different L shells with GOES East typically being of the order of $0.2L$ farther from the Earth. Since the radial gradient of flux is generally outward near geosynchronous orbit, GOES West will typically measure larger fluxes than GOES East [*Onsager et al.*, 2004] and our analysis shows that on average, this difference in L results in a factor of ~2.5 difference between the daily averaged fluxes measured at GOES West and GOES East, with the larger fluxes being measured at GOES West.

Koons [2001] conducted an extreme value analysis of the GOES $E > 2$ MeV electron flux covering the period from 1 January 1986 to 31 August 1999. This study combined data from two versions of the $E > 2$ MeV detector and did not correct the data for dead time. The earlier version, which was used on satellites prior to GOES 8, suffered from dose damage which resulted in larger flux differences between GOES 5, 6, and 7 than those on GOES 8 and beyond [*Su et al.*, 2014]. Furthermore, the *Koons* [2001] study combined data from different longitudes, which could affect the results by a factor of 2, depending on satellite location. With these caveats in mind it is informative to compare our findings with those of *Koons* [2001].

The N year event levels calculated by *Koons* [2001] are tabulated in Table 3 together with the new results presented here. Our return levels are generally larger than those presented in *Koons* [2001]. For example, the 1 in 10 year flux at GOES West (East) determined here is about a factor of 2.7 (1) times that estimated from the *Koons* [2001] study. For more extreme events, the 1 in 100 year flux at GOES West (East) determined here is about a factor of 7 (3) times that estimated by *Koons* [2001].

Our analysis suggests that there is no upper limit to the maximum expected flux. This is in contrast to the work of *Koons* [2001] who suggests that the fluxes tend to an upper limit of 2.34×10^5 cm^{-2} s^{-1} sr^{-1}. The different conclusion regarding the presence or absence of an upper flux limit could be due to the inclusion of satellite data prior to GOES 8 or the mixing of the data from different longitudes. More recently, *O'Brien et al.* [2007] inferred an upper limit to the energetic electron fluxes over a broad range of energies and L shells including geosynchronous orbit using data from the Los Alamos National Laboratory sensors between 1989 and 2005. Both studies used log fluxes since there is considerable uncertainty in the shape parameter. We repeated our study using log fluxes and determined values for the shape parameter of 0.019 ± 0.28 and 0.16 ± 0.23 for GOES West and GOES East, respectively. The shape parameter is thus still

Table 3. Comparison of *N* Year Event Levels With *Koons* [2001]

Event	GOES West (cm^{-2} s^{-1} sr^{-1})	GOES East (cm^{-2} s^{-1} sr^{-1})	*Koons* [2001] (cm^{-2} s^{-1} sr^{-1})
1 in 10 years	1.84×10^5	6.53×10^4	6.78×10^4
1 in 20 years	2.83×10^5	1.04×10^5	7.98×10^4
1 in 50 years	5.00×10^5	1.98×10^5	9.57×10^4
1 in 100 years	7.68×10^5	3.25×10^5	1.08×10^5
1 in 150 years	9.86×10^5	4.35×10^5	1.15×10^5

positive, and the results of the linear flux fit lie within the range of the results of the log flux fit. However, the shape parameter for both log flux fits includes negative values within their error bars suggesting that we treat the conclusion that the fluxes have no upper bound with caution. In reality, there is likely to be an upper limit set by some physical process, but this is not evident from the statistical analysis here. The results demonstrate the difficulty of conclusively determining the presence or absence of an upper bound from 10 to 20 years of data. A definitive answer will require substantially more data covering a much longer period of time.

The largest space weather event of the last 200 years is widely accepted to be the Carrington event of 1859. Indeed, when ranked by five different space weather effects, the Carrington event is the only event to appear at or near the top of each ranking [*Cliver and Svalgaard*, 2004]. Historical auroral records suggest that the return period of Carrington-level events is 150 years [*Lloyd's*, 2013]. From our study, the return levels for a 150 year event, i.e., similar in frequency to a Carrington-level event, are 9.86×10^5 and 4.35×10^5 cm^{-2} s^{-1} sr^{-1} for GOES West and GOES East, respectively.

The largest flux observed in the 19.5 year period between January 1995 and June 2014, of 4.92×10^5 cm^{-2} s^{-1} sr^{-1} , was recorded by GOES 10 operating at the GOES West position on 29 July 2004. Our analysis shows that this point lies just inside the 95% confidence limit. The largest flux recorded at GOES East, of 1.93×10^5 cm^{-2} s^{-1} sr^{-1}, also occurred on 29 July and lies just outside the 95% confidence limit. The fact that this extreme flux was recorded by two independent satellites suggests that it is real. From the return plots for the GOES West and GOES East data, shown in Figures 6d and 7d, respectively, it can be seen that the observed maximum fluxes would only be expected to be seen once in every 50 years, suggesting that the event on 29 July 2004 was a 1 in 50 year event.

It is informative to look at this event in more detail to see what factors may have led to such an extreme value. The IMF *Bz* remained southward for significant periods during the recovery phase of each of the storms, remaining predominantly southward for 14 h, 10 h, and 43 h for the first, second, and third storm recovery phases, respectively. Predominantly southward IMF *Bz* during the storm recovery phase is known to be an important requirement for efficient electron acceleration to relativistic energies [*Iles et al.*, 2002; *Miyoshi and Kataoka*, 2008; *Miyoshi et al.*, 2013]. For the first and second storms the average values of the *AE* index during the 14 and 10 h of predominantly southward IMF *Bz* were 968 and 893 nT, respectively. For the third storm, the average value of the *AE* index was 870 nT for the first 10 h following the *Dst* minimum and 341 nT for the next 33 h. Such high and sustained levels of *AE*, driven by the southward IMF *Bz*, are likely to be associated with strong and sustained levels of whistler mode chorus [*Meredith et al.*, 2001, 2012; *Li et al.*, 2009, 2011; *Miyoshi et al.*, 2013] and seed electrons [*Meredith et al.*, 2003; *Miyoshi et al.*, 2013] and concomitant acceleration of the seed electrons to MeV energies by resonant wave-particle interactions with the whistler mode chorus waves [e.g., *Horne et al.*, 2005a, 2005b]. Furthermore, during the recovery phase of the third storm the solar wind pressure stayed low, $<$ 1.0 nPa, for a few days leading to an expanded magnetosphere aiding the magnetic confinement of the freshly generated radiation belt relativistic electrons [*Kataoka and Miyoshi*, 2008b]. Detailed modeling of this event is now required to see if the extreme flux levels observed can be captured by current radiation belt models.

Following the third storm on 27 July 2004, the $E > 2$ MeV flux was elevated for a period of 10 days. We might therefore expect to find some evidence of anomaly increases during this period. Indeed, Double Star TC1 and TC2 reported over 30 anomalies during the period from July 27 to 10 August 2004, the majority of which occurred in the Earth's radiation belt and were attributed to internal charging [*Han et al.*, 2005]. Furthermore, on 3 August 2004, during the period when the relativistic electron fluxes were enhanced, Galaxy 10R lost its secondary xenon ion propulsion system, used to maintain its in-orbit position, reducing its lifetime

significantly [*Choi et al.*, 2011] and resulting in an insurance payout of U.S. $75.3 million [*Seradata SpaceTrak Launch and Satellite Database*, www.seradata.com]. The satellite, which was launched in January 2000 and had been expected to last for 15 years, was eventually decommissioned in 2008.

The results suggest that satellites in geosynchronous orbit will be most prone to radiation damage when they are located near the magnetic equator and least prone to radiation damage when they are located farthest from the magnetic equator. Geosynchronous satellites located near 20°E and 160°W will thus on average experience the largest fluxes, while those located near 110°E and 70°W will, on average, receive the least. It is interesting to note that the difference in the average flux levels experienced at GOES East and GOES West is about the same as the difference between a 1 in 10 and a 1 in 50 year events at either location so that a 1 in 50 year event at GOES East is approximately equal to a 1 in 10 year event at GOES West.

7. Conclusions

We have conducted an extreme value analysis of daily averaged $E > 2$ MeV electron fluxes from the GOES satellites during the 19.5 year period from 1 January 1995 to 30 June 2014. Due to gaps in satellite coverage and careful selection of data, this results in 16 and 15.5 years of good quality operational data at GOES West and GOES East, respectively. Our principal results are as follows:

1. The daily averaged flux of $E > 2$ MeV electrons measured at GOES West is typically a factor of ~2.5 higher than that measured at GOES East.
2. The 1 in 10, 1 in 50, 1 in 100, and 1 in 150 year daily averaged $E > 2$ MeV electron fluxes at GOES West are 1.84×10^5, 5.00×10^5, 7.68×10^5, and 9.86×10^5 cm^{-2} s^{-1} sr^{-1}, respectively. The corresponding 1 in 10, 1 in 50, 1 in 100, and 1 in 150 year fluxes at GOES East are 6.53×10^4, 1.98×10^5, 3.25×10^5, and 4.35×10^5 cm^{-2} s^{-1} sr^{-1}.
3. We suggest that the flux of $E > 2$ MeV electrons measured at GOES West is higher than that measured at GOES East because the satellite at GOES West is at a lower magnetic latitude and hence L shell. Thus, geosynchronous satellites located near 20°E and 160°W will, on average, experience the largest fluxes.
4. The largest event seen during the 19.5 year period on 29 July 2004 was a particularly extreme event and was seen by satellites at GOES West and GOES East. The extreme value analysis suggests that this event was a 1 in 50 year event.

We caution that the relationship between satellite anomalies and high levels of relativistic electron flux is complex and there is no one to one correspondence. Additional factors such as the timescale for charging and decay of the dielectrics are likely to play an additional important role [*Bodeau*, 2010].

Appendix A: Cross Comparisons of the GOES $E > 2$ MeV Relativistic Electron Channel

The effect of different energetic particle sensor sensitivities on the observed ratios of the GOES West to the GOES East fluxes needs to be determined. To this end, we apply a modified version of the method first devised by *Onsager et al.* [2004] to compare the GOES 8 and GOES 9 $E > 2$ MeV electron fluxes. This method takes advantage of situations in which two GOES satellites are separated by approximately 1 h in local time, a condition that has existed on several occasions for extended periods, or when there is a near conjunction in the course of a station change. The small physical separation reduces differences due to different geomagnetic latitudes. The time separation is corrected for by shifting one time series in time before comparing it to the other. This approach is valid when electron drift paths are undisturbed by local time-dependent effects such as substorms; therefore, we apply the condition that the *Kp* index be less than 2 in order to reduce scatter in the cross comparisons. For the satellites used in this study, we have identified four occasions according to the above criteria that permit an accurate cross comparison and one occasion that is of lower quality though still useful. The cross comparisons performed for this paper are summarized in Table A1. The labels "w" and "e" in the last two rows indicate the instrument look direction during the indicated period.

Following *Rodriguez et al.* [2014], the relationship between the two time series adjusted as described above is fit to a linear model, $j_y = A_1 j_x + A_0$, using a least absolute deviation fit, and the standard errors of the fit parameters, σ_1 and σ_0, are calculated using a Monte Carlo bootstrap method with replacement [*Efron and*

Table A1. Results of Cross Comparisons of the GOES *E*2 ($E > 2$ MeV) Relativistic Electron Channel, for $Kp < 2$[a]

Sat *y*	Sat *x*	Period	Separation LT (h)	A_1	σ_1	A_0 (cm^{-2} s^{-1} sr^{-1})	σ_0 (cm^{-2} s^{-1} sr^{-1})	r^2	*N*
9	8	Jul–Nov 1995	0.95–1.08	1.0477	0.0039	−2.0573	0.1864	0.9789	23073
10	9	Jul 1998	1.63–2.12	0.6845	0.0063	1.2328	0.4673	0.9621	2956
11	10	Jun–Aug 2006	−1.0–1.0	0.8067	0.0062	30.033	2.4416	0.9502	8432
10	12	Jan–May 2007	0.95–1.15	0.8805	0.0041	−2.8030	0.6656	0.9551	25606
15w	13w	Apr–Aug 2011	0.88–1.04	1.2301	0.0033	0.7523	0.3858	0.9893	15067
15e	13w	Apr–Aug 2011	0.88–1.04	1.0024	0.0026	0.1177	0.2889	0.9892	15067

[a] $A_1\ (10-8) = A_1\ (10-9) \times A_1\ (9-8) = 0.7172$; $A_1\ (11-12) = A_1\ (11-10) \times A_1\ (10-12) = 0.7103$.

Tibshirani, 1986]. The fraction of the variance explained by the linear model, r^2, is also calculated. If A_1 is less than 1, then an uncorrected west-to-east ratio with j_y in the numerator and j_x in the denominator is an underestimate of the true ratio by a factor A_1.

The comparison between GOES 8 and 9 is expanded from 3 days (3–5 July 1995) as in *Onsager et al.* [2004] to all times with $Kp < 2$ during July–November 1995. A 5 month period is also used for the GOES 12 versus 10 and GOES 13 versus 15 comparisons. In these three cases, which correspond directly to three of the GOES West to East comparisons in this paper, the satellites were separated by approximately 1 h. In the case of GOES 15, both detectors look westward at some point during the period of interest [*Rodriguez et al.*, 2014]; therefore, results are given of cross comparisons between the westward looking GOES 13 detector and both GOES 15 detectors.

For the remaining GOES East versus West comparisons (8 versus 10 and 12 versus 11), no direct cross comparisons are possible between the two satellites. However, a transfer of cross comparisons is possible from GOES 10 to 9 to 8 and from GOES 11 to 10 to 12. At the end of June 1998, GOES 9 went into storage mode and data taking ceased prior to a near conjunction with GOES 10, so we have to compare measurements made when the two satellites were separated by 1.63–2.12 h in local time, greater than the preferred 1 h criterion of *Onsager et al.* [2004]. Since GOES 10 was east of GOES 9 during June 1998, the observed 31.5% discrepancy ($A_1 = 0.6845$) between GOES 10 and GOES 9, the largest observed in these cross comparisons, is probably larger than the true difference in sensitivity between the two instruments. In 2006, GOES 10 and 11 had a near conjunction at the end of June; the cross comparison is performed over the period before and after the near conjunction when they were within 1 h of each other. The results of the cross-comparison transfers are given as footnotes in Table A1.

Based on these cross comparisons, the observed (uncorrected) west-to-east $E > 2$ MeV electron flux ratios range from a 29% underestimate (GOES 11 to 12) to a 23% overestimate (GOES 15 to 13). Therefore, the differences in response between the various $E > 2$ MeV channels are much less than the systematic factor of ~2.5 between the GOES West and GOES East fluxes.

Acknowledgments
We thank T. Onsager and A. Newman for providing the count rates from the earlier GOES satellites in support of the dead time correction calculation. We also thank the Satellite Situation Center Web (SSCWeb) at NASA Goddard Space Flight Center for making the satellite locations available and the NSSDC Omniweb for provision of the geomagnetic indices. This study is part of the British Antarctic Survey Polar Science for Planet Earth program. The research leading to these results has received funding from the Natural Environment Research Council and the European Union Seventh Framework Programme (FP7/2007-2013) under grant agreement 606716 (SPACESTORM). J.V.R. was supported by NGDC Task II under the CIRES Cooperative Agreement between NOAA and the University of Colorado. The data used to generate the plots in this paper are stored at the BAS Polar Data Centre and are available on request.

References

Adams, J. H., A. A. Beliaev, N. V. Kuznetsov, R. A. Nymmik, and E. C. Smith (1996), Occurrence frequency of single event upsets induced on geosynchronous orbit: Model calculations and TDRS-1 experience, *Radiat. Meas.*, *26*, 509–512.

Allen, J. (2010), The Galaxy 15 anomaly: Another satellite in the wrong place at a critical time, *Space Weather*, *8*, S06008, doi:10.1029/2010SW000588.

Baker, D. N. (2001), Satellite anomalies due to space storms, in *Space Storms and Space Weather Hazards*, edited by I. A. Daglis, pp. 285–311, Springer, New York.

Baker, D. N., J. B. Blake, L. B. Callis, J. R. Cummings, D. Hovestadt, S. Kanekal, B. Klecker, R. A. Mewaldt, and R. D. Zwickl (1994), Relativistic electron acceleration and decay time scales in the inner and outer radiation belts: SAMPEX, *Geophys. Res. Lett.*, *21*(6), 409–412, doi:10.1029/93GL03532.

Baker, D. N., S. G. Kanekal, R. B. Horne, N. P. Meredith, and S. A. Glauert (2007), Low-altitude measurements of 2–6 MeV electron trapping lifetimes at $L \leq L \leq 2.5$, *Geophys. Res. Lett.*, *34*, L20110, doi:10.1029/2007GL031007.

Blake, J. B., W. A. Kolasinski, R. W. Fillius, and E. G. Mullen (1992), Injection of electrons and protons with energies of tens of MeV into $L < 3$ on 24 March 1991, *Geophys. Res. Lett.*, *19*(8), 821–824.

Bodeau, M. (2010), High energy electron climatology that supports deep charging risk assessment in GEO, paper presented at 48th AIAA Aerospace Sciences Meeting Including the New Horizons Forum and Aerospace Exposition, Orlando, Fla., 4–7 Jan.

Cabinet Office (2012), *National Risk Register of Civil Emergencies*, Cabinet Office, 70 Whitehall, London. [Available at www.cabinetoffice.gov.uk.]

Cayton, T. E., R. D. Belian, S. P. Gary, T. A. Fritz, and D. N. Baker (1989), Energetic electron components at geosynchronous orbit, *Geophys. Res. Lett.*, *16*(2), 147–150, doi:10.1029/GL016i002p00147.

Choi, H.-S., J. Lee, K.-S. Cho, Y.-S. Kwak, I.-H. Cho, Y.-D. Park, Y.-H. Kim, D. N. Baker, G. D. Reeves, and D.-K. Lee (2011), Analysis of GEO spacecraft anomalies: Space weather relationships, *Space Weather*, *9*, S06001, doi:10.1029/2010SW000597.

Cliver, E. W., and L. Svalgaard (2004), The 1859 solar-terrestrial disturbance and the current limits of extreme space weather activity, *Sol. Phys.*, *224*, 407–422.

Coles, S. (2001), *An Introduction to Statistical Modelling of Extreme Values*, Springer, London.

Dacheva, T. P., B. T. Tomova, Y. N. Matviichuka, P. G. Dimitrova, N. G. Bankova, G. Reitzb, G. Horneckb, D. P. Häderc, M. Lebertd, and M. Schusterd (2013), Relativistic electron fluxes and dose rate variations observed on the international space station, *J. Atmos. Sol. Terr. Phys.*, *99*, 150–156.

Della-Marta, P. M., H. Mathis, C. Frei, M. A. Liniger, J. Kleinn, and C. Appenzeller (2009), The return period of wind storms over Europe, *Int. J. Climatol.*, *29*, 437–459, doi:10.1002/joc.1794.

Efron, B., and R. Tibshirani (1986), Bootstrap methods for standard errors, confidence intervals, and other measures of statistical accuracy, *Stat. Sci.*, *1*, 54–77.

Gubby, R., and J. Evans (2002), Space environment effects and satellite design, *J. Atmos. Solar Terr. Phys.*, *64*, 1723–1733.

Han, J., J. Huang, Z. Liu, and S. Wang (2005), Correlation of Double Star anomalies with space environment, *J. Spacecr. Rock.*, *42*, 1061–1065, doi:10.2514/1.14773.

Hanser, F. A. (2011), EPS/HEPAD calibration and data handbook, *Tech. Rep. GOESN-ENG-048D*, Assurance Technology Corporation, Carlisle, Mass. [Available at http://www.ngdc.noaa.gov/stp/satellite/goes/documentation.html.]

Heffernan, J. E., A. G. Stephenson, and E. Gilleland (2014), *ISMEV: An Introduction to Statistical Modeling of Extreme Values, Version 1.39*, Springer, London. [Available at http://www.ral.ucar.edu/ericg/softextreme.php.]

Horne, R. B. (2002), The contribution of wave-particle interactions to electron loss and acceleration in the Earth's radiation belts during geomagnetic storms, in *URSI Review of Radio Science 1999–2002*, edited by W. R. Stone, pp. 801–828, Wiley, Hoboken, N. J.

Horne, R. B., et al. (2005a), Wave acceleration of electrons in the Van Allen radiation belts, *Nature*, *437*, 227–230, doi:10.1038/nature03939.

Horne, R. B., R. M. Thorne, S. A. Glauert, J. M. Albert, N. P. Meredith, and R. R. Anderson (2005b), Timescale for radiation belt electron acceleration by whistler mode chorus waves, *J. Geophys. Res.*, *110*, A03225, doi:10.1029/2004JA010811.

Horne, R. B., S. A. Glauert, N. P. Meredith, D. Boscher, V. Maget, D. Heynderickx, and D. Pitchford (2013), Space weather impacts on satellites and forecasting the Earth's electron radiation belts with SPACECAST, *Space Weather*, *11*, 169–186, doi:10.1002/swe.20023.

ICRU (1994), Particle counting in radioactivity measurements, *Tech. Rep. 52*, International Commission on Radiation Units and Measurements (ICRU), Bethesda, Md.

Iles, R. H. A., A. N. Fazakerley, A. D. Johnstone, N. P. Meredith, and P. Buhler (2002), The relativistic electron response in the outer radiation belt during magnetic storms, *Ann. Geophys.*, *20*, 957–965.

Iucci, N., et al. (2005), Space weather conditions and spacecraft anomalies in different orbits, *Space Weather*, *3*, S01001, doi:10.1029/2003SW000056.

Kataoka, R., and Y. Miyoshi (2008a), Magnetosphere inflation during the recovery phase of geomagnetic storms as an excellent magnetic confinement of killer electrons, *Geophys. Res. Lett.*, *35*, L06S09, doi:10.1029/2007GL031842.

Kataoka, R., and Y. Miyoshi (2008b), Average profiles of the solar wind and the outer radiation belt during the extreme flux enhancement of relativistic electrons at geosynchronous orbit, *Ann. Geophys.*, *26*, 1335–1339.

Knoll, G. F. (2000), *Radiation Detection and Measurement*, 3rd ed., Wiley, Univ. of Mich., Ann Arbor.

Koons, H. C. (2001), Statistical analysis of extreme values in space science, *J. Geophys. Res.*, *106*(A6), 10,915–10,921, doi:10.1029/2000JA000234.

Koons, H. C., and J. F. Fennell (2006), Space weather effects on communications satellites, *Radio Sci. Bull. Int. Union Radio Sci. (URSI)*, *316*, 27–41.

Krausmann, E. (2011), The space-weather awareness dialogue: Findings and outlook, *JRC Scientific and Technical Reports*, Brussels, Belgium, 25–26 Oct.

Lanzerotti, L. J., C. Breglia, D. W. Maurer, G. K. Jonson III, and C. G. Maclennan (1998), Studies of spacecraft charging on a geosynchronous telecommunications satellite, *Adv Space Res.*, *22*, 79–82.

Li, W., R. M. Thorne, V. Angelopoulos, J. Bortnik, C. M. Cully, B. Ni, O. LeContel, A. Roux, U. Auster, and W. Magnes (2009), Global distribution of whistler-mode chorus waves observed on the THEMIS spacecraft, *Geophys. Res. Lett.*, *36*, L09104, doi:10.1029/2009GL037595.

Li, W., J. Bortnik, R. M. Thorne, and V. Angelopoulos (2011), Global distribution of wave amplitudes and wave normal angles of chorus waves using THEMIS wave observations, *J. Geophys. Res.*, *116*, A12205, doi:10.1029/2011JA017035.

Li, Y., W. Cai, and E. P. Campbell (2005), Statistical Modeling of extreme rainfall in southwest Western Australia, *J. Clim.*, *18*, 852–863.

Lloyd's (2013), *Solar Storm Risk to the North American Electric Grid*, Report by Lloyds and the Atmospheric and Environmental Research, Inc., London. [Available at http://www.lloyds.com/news-and-insight/risk-insight/library/natural-environment/solar-storm], accessed on 7 August.

Meredith, N. P., R. B. Horne, and R. R. Anderson (2001), Substorm dependence of chorus amplitudes: Implications for the acceleration of electrons to relativistic energies, *J. Geophys. Res.*, *106*, 13,165–13,178.

Meredith, N. P., M. Cain, R. B. Horne, R. M. Thorne, D. Summers, and R. R. Anderson (2003), Evidence for chorus driven electron acceleration to relativistic energies from a survey of geomagnetically disturbed periods, *J. Geophys. Res.*, *108*(A6), 1248, doi:10.1029/2002JA009764.

Meredith, N. P., R. B. Horne, A. Sicard-Piet, D. Boscher, K. H. Yearby, W. Li, and R. M. Thorne (2012), Global model of lower band and upper band chorus from multiple satellite observations, *J. Geophys. Res.*, *117*, A12209, doi:10.1029/2012JA017978.

Miyoshi, Y. S., V. K. Jordanova, A. Morioka, and D. S. Evans (2004), Solar cycle variations of the electron radiation belts: Observations and radial diffusion simulation, *Space Weather*, *2*, S10S02, doi:10.1029/2004SW000070.

Miyoshi, Y., and R. Kataoka (2008), Flux enhancement of the outer radiation belt electrons after the arrival of stream interaction regions, *J. Geophys. Res.*, *113*, A03S09, doi:10.1029/2007JA012506.

Miyoshi, Y., R. Kataoka, Y. Kasahara, A. Kumamoto, T. Nagai, and M. F. Thomsen (2013), High-speed solar wind with southward interplanetary magnetic field causes relativistic electron flux enhancement of the outer radiation belt via enhanced condition of whistler waves, *Geophys. Res. Lett.*, *40*, 4520–4525, doi:10.1002/grl.50916.

Nogaj, M., P. Yiou, S. Parey, F. Malek, and P. Naveau (2006), Amplitude and frequency of temperature extremes over the North Atlantic region, *Geophys. Res. Lett.*, *33*, L10801, doi:10.1029/2005GL024251.

O'Brien, T. P., J. F. Fennell, J. L. Roeder, and G. D. Reeves (2007), Extreme electron fluxes in the outer zone, *Space Weather*, *5*, S01001, doi:10.1029/2006SW000240.

Odenwald, S. F., and J. L. Green (2007), Forecasting the impact of an 1859-caliber superstorm on geosynchronous Earth-orbiting satellites: Transponder resources, *Space Weather*, *5*, S06002, doi:10.1029/2006SW000262.

Onsager, T. G., R. Grubb, J. Kunches, L. Matheson, D. Speich, R. Zwickl, and H. Sauer (1996), Operational uses of the GOES energetic particle detectors, in GOES-8 and beyond, *Proc. SPIE Int. Soc. Opt. Eng.*, *2812*, 281–290.

Onsager, T. G., A. A. Chan, Y. Fei, S. R. Elkington, J. C. Green, and H. J. Singer (2004), The radial gradient of relativistic electrons at geosynchronous orbit, *J. Geophys. Res.*, *109*, A05221, doi:10.1029/2003JA010368.

Picklands, J. (1975), Statistical inference using extreme order statistics, *Ann. Stat.*, *3*, 119–131.

R Development Core Team (2008), *R: A Language and Environment for Statistical Computing*, R Foundation for Statistical Computing, Vienna, Austria. [Available at http://www.R-project.org.]

Rodriguez, J. V., J. C. Krosschell, and J. C. Green (2014), Intercalibration of GOES 8–15 solar proton detectors, *Space Weather*, *12*, 92–109, doi:10.1002/2013SW000996.

Royal Academy of Engineering Report (2013), *Extreme Space Weather: Impacts on Engineered Systems and Infrastructure*, Royal Acad. of Eng., London.

Su, Y.-J., J. M. Quinn, W. R. Johnston, J. P. McCollough, and M. J. Starks (2014), Specification of $>$ 2 MeV electron flux as a function of local time and geomagnetic activity at geosynchronous orbit, *Space Weather*, *12*, 470–486, doi:10.1002/2014SW001069.

Tebaldi, C., B. H. Strauss, and C. E. Zervas (2012), Modelling sea level rise impacts on storm surges along U.S. coasts, *Environ. Res. Lett.*, *7*, 14,032, doi:10.1088/1748-9326/7/1/014032.

Thomson, A. W. P., E. B. Dawson, and S. J. Reay (2011), Quantifying extreme behavior in geomagnetic activity, *Space Weather*, *9*, S10001, doi:10.1029/2011SW000696.

Thorne, R. M. (2010), Radiation belt dynamics: The importance of wave-particle interactions, *Geophys. Res. Lett.*, *37*, L22107, doi:10.1029/2010GL044990.

Van Allen, J. A., and L. A. Frank (1959), Radiation around the Earth to a radial distance of 107,400 km, *Nature*, *183*, 430–434.

Viereck, R. (2012), The U.S.-UK Space Weather Workshop, *Space Weather*, *10*, S04002, doi:10.1029/2011SW000770.

Webb, F. D., and J. H. Allen (2004), Spacecraft and ground anomalies related to the October–November 2003 solar activity, *Space Weather*, *2*, S03008, doi:10.1029/2004SW000075.

Wilkinson, D. C., S. C. Daughtridge, J. L. Stone, H. H. Sauer, and P. Darling (1991), TDRS-1 single event upsets and the effect of the space environment, *IEEE Trans. Nucl. Sci.*, *38*, 1708–1712.

Wrenn, G. L. (1995), Conclusive evidence for internal dielectric charging anomalies on geosynchronous communications spacecraft, *J. Spacecr. Rockets*, *32*, 514–520.

Wrenn, G. L., D. J. Rodgers, and K. A. Ryden (2002), A solar cycle of spacecraft anomalies due to internal charging, *Ann. Geophys.*, *20*, 953–956.